COBEM 2021 26th International Congress of Mechanical Engineering
November 22-26, 2021, Virtual Congress, Brazil

COB-2021-0473
INLFUENCE OF SPIF PARAMETERS ON DRY INCREMENTAL FORMING OF TITANIUM SHEETS FOR BIOMEDICAL APPLICATIONS AND SURFACE COMPARISON AGAINST COMMERCIAL HIP IMPLANT

Felipe dos Anjos Rodrigues Campos
Leonardo Rosa Ribeiro da Silva
Federal University of Uberlândia-UFU, LEPU, 2121 João Naves de Ávila avenue, Uberlândia-MG, Brazil
filipin_anjos@hotmail.com ; leonardo.rrs@gmail.com

Pedro Henrique Pires França
Federal University of Uberlândia-UFU, LEPU, 2121 João Naves de Ávila avenue, Uberlândia-MG, Brazil
pedrohenriquepiresf96@gmail.com

Weber Sebastião da Silva
UNA University Center, 59 Paulina Margonari street, Uberlândia-MG, Brazil
weber_silva23@hotmail.com

Abstract. *Single Point Incremental Forming (SPIF) stands out as a non-conventional technology for producing stamped final parts from thin metal sheets without the use of expensive tooling. This is of special interest for production of custom biomedical parts, as long as the process parameters are correctly adjusted to guarantee adequate surface characteristics. In this work, SPIF was carried on titanium sheets under 7 different conditions. The roughness was assessed by different parameters, while SEM images and chemical analysis by EDS were used to compare the surface aspect to that of a commercial hip implant. While the Ra was still larger than recommended in the literature, it was lower than that of the plasma sprayed femoral component of the validated hip implant. This product and the cones produced in lubricated SPIF tests predominantly present regularly spaced peaks, while the dry tests yielded surfaces with slightly more valleys. Despite the uneven distribution of titanium oxide fragments on the surface and lower amount compared to the plasma sprayed femoral component, these structures are still present, which guarantees the biocompatibility of the formed parts and indicate the ability of the SPIF process to produce ready to use biomedical parts.*

Keywords: *Single Point Incremental Forming, titanium, roughness, morphological space, biocompatibility*

1. INTRODUCTION

The accelerated evolution of rapid prototyping processes in recent years has contributed significantly to biomedical industry, mainly due to the easiness in producing customized parts according to patient's needs. In this regard, incremental sheet forming stands out as a non-conventional technology for producing stamped final parts from thin metal sheets without the use of expensive tooling (Oliveira et. al., 2018). The most common configuration is known as Single Point Incremental Forming (SPIF) and consists of using a CNC machine to drive a cylindrical tool of spherical head against the flat sheet in a defined pathway, increasing the depth in each pass, as shown in Fig. 1.

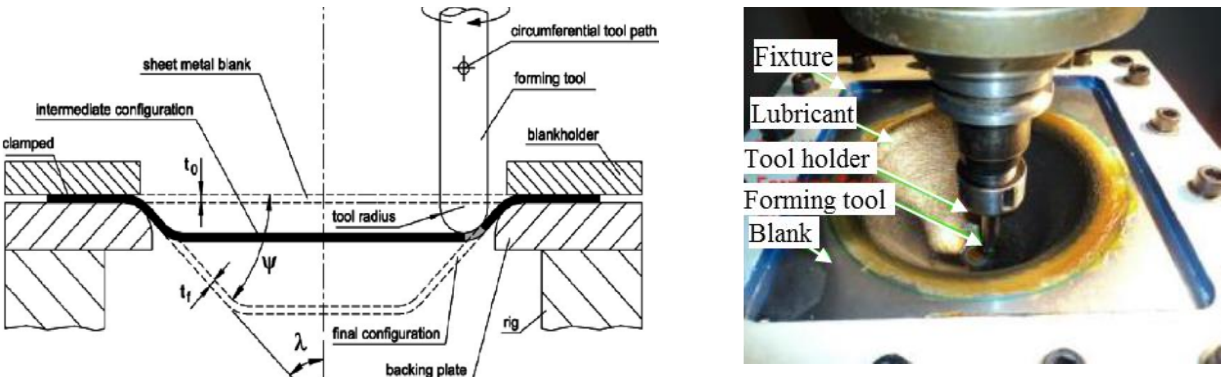

(a) (b)

Figure 1. Positioning of plate and tool on a CNC machine for SPIF process. Adapted from Doss et. al. (2013).

The most important process parameters are the tool rotation and feed, vertical step, wall angle and lubrication, which might have different effects on surface integrity, mechanical resistance and geometrical conformity depending on the sheet material and friction at the tool-sheet interface (Mateus et. al., 2019). Additionally, the complex combination of plastic deformation, bending effect and sheet thinning makes this process hard to model, so that parameters must be finely adjusted to optimize the characteristics of the final part. For instance, Gandla et. al. (2020) performed aluminum stamping and observed an increase in the Ra parameter with the vertical step, and its decrease when the wall angle and tool diameter were raised, although this behavior can change depending on the sheet material and thickness. On the other side, Cheng et. al. (2020) found that the finish depends mainly on friction at the interface with the tool and the roughness of the tool itself.

At first, most studies on surface finish in incremental stamping focus on reducing part roughness, whether by lubrication, tool surface conditioning or adjustment of process parameters. However, from a biomedical point of view, micrometric imperfections can be beneficial in the case of orthopedic implants. Civantos et. al. (2019) performed in vitro cell growth tests on parts manufactured by powder metallurgy, showing greater proliferation in more porous parts with Ra in the range of 3 to 10 µm when compared to the solid part with Ra roughness equal to 0.7 µm . In addition, blasting or chemical attack techniques are also favorable for amplifying cell adhesion sites, as shown in the in vivo tests by Hacking et. al. (2012).

In this type of application, the most used material is titanium, thanks to its good mechanical properties and excellent corrosion resistance. In addition, the titanium dioxide layer that naturally forms on the surface also induces bone cell adhesion and proliferation, accelerating patient recovery (Chen et. al., 2020). Although the exact mechanism is not yet fully understood, chemical interactions of TiO_2 with calcium ions in the bone matrix attract proteins that stimulate the multiplication and differentiation of osteoblasts, the young bone cells. For this reason, several treatments are carried out in order to increase the proportion of this oxide on the implant surface, such as plasma oxygenation and electrolytic deposition, or supersonic blasting on other materials (Agarwal and García, 2015).

In this sense, it would be beneficial to adjust the parameters of SPIF to produce titanium parts with surface suitable for use as implants without the need of further treatments. This work investigated the influence of dry SPIF process parameters on surface roughness and chemical composition, comparing it to results obtained in lubricated SPIF trials and to the surface of a commercial hip implant. Although the later may not be the most suitable comparison since it is a surface treatment process instead of forming method, it serves as an important benchmark when assessing surface chemistry and roughness regarding osseointegration of orthopedic and cranial implants. Stamping tests were performed under different conditions of rotation, feed and vertical step to produce straight cones. Chemical composition analysis was performed by energy dispersion X-ray spectroscopy and the surface appearance was visualized in the Scanning Electron Microscope. Roughness was measured in a contact rugosimeter and evaluated not only by the traditional Ra parameter, but also by observing the morphological space characterized by skewness and kurtosis.

2. METHODOLOGY

The SPIF tests were performed under dry condition with 1 mm thick pure titanium sheets, varying the vertical step, tool rotation and feed, as shown in Table 1. For comparison, the process parameters of lubricated tests studied by Campos et. al. (2021) have also been exhibited. Tools of semi-spherical point with diameter 10 mm were employed, turned from cylindrical steel bars SAE 52100. The tests were carried out in a ROMI Bridgeport 760 universal machining center with 9 kW maximum power, and a cast iron support was used for fixing the sheets. The tool's helical path was exported from the CAD-CAM interface of the software Solidworks 2018. The equipment was adjusted for the production of straight cones with a wall angle of 45° and a base diameter of 80 mm, shown in Fig. 2(a). Figure 2(b) shows the femoral component of the commercial hip implant used as benchmark.

Table 1. Parameters of SPIF trials for production of straight titanium cones with wall angle of 45°.

Test	**Tool rotation/speed (V)**		**Tool feed (f)**	**Vertical step (p)**	**Lubrication (L)**
	[rpm]	**[m/min]**	**[m/min]**	**[mm]**	
1	75 (V-)	2.36	800 (f-)	0,8 (p+)	oil
2	150 (V+)	4.71	800 (f-)	0,5 (p-)	oil
3	75 (V-)	2.36	1200 (f+)	0,5 (p-)	oil
4	150 (V+)	4.71	1200 (f+)	0,8 (p+)	oil
5	10 (V-)	0.31	800 (f-)	0,5 (p-)	-
6	10 (V-)	0.31	1200 (f+)	0,5 (p-)	-
7	10 (V-)	0.31	800 (f-)	0,8 (p+)	-

The rough surface of the cones and implant were observed in a Scanning Electron Microscope (SEM) Zeiss EVO MA10, and chemical composition was assessed through Energy Dispersion X-Ray Spectroscopy (EDS) with a detector Oxford INCAx-act. Roughness measurements were carried using a Taylor Hobson Surtronic S-100 contact roughness

meter, with a resolution of 0.01 µm. The 2.5 mm cut-off and Gaussian filter were used as recommended by ISO 4288 (2008), to perform four equally spaced measurements on the rough surfaces of SPIF parts and femoral component.

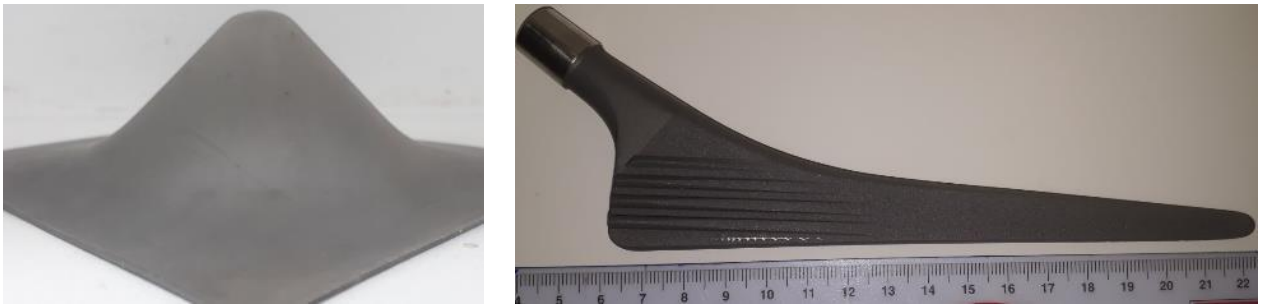

(a) (b)

Figure 2. (a) Titanium cones obtained by dry SPIF, showing external surface. (b) Femoral component of commercial hip implant used as comparison for surface roughness and chemical composition.

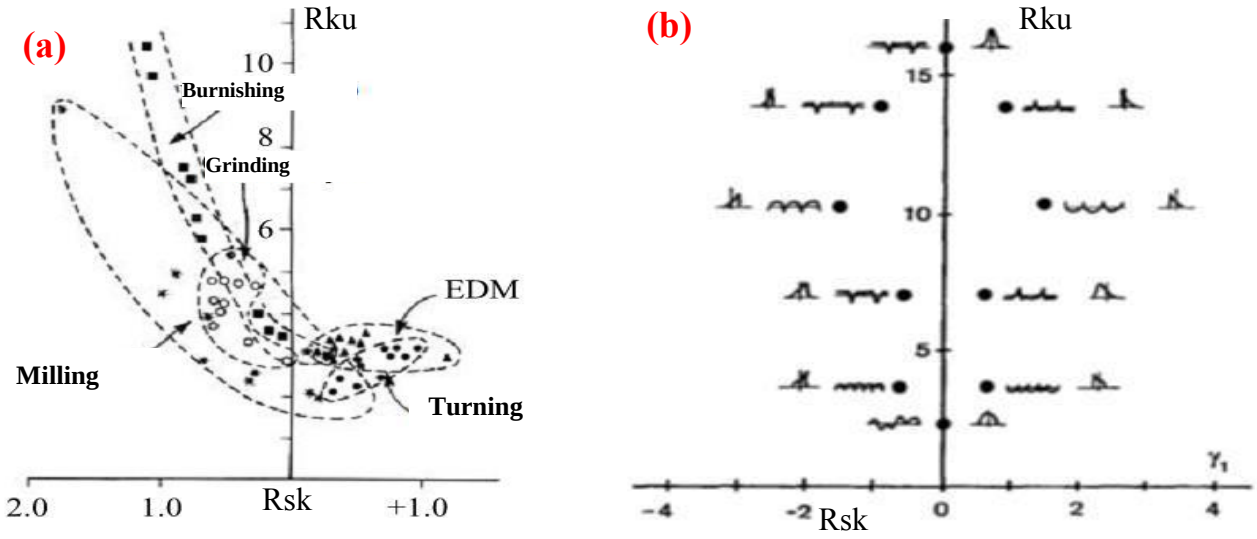

Figure 3. (a) Representation of the morphological space of the different manufacturing processes. (b) Examples of profiles according to the region of the morphological space. Adapted from Mezari (2013).

Table 2. Definition of roughness parameters used in the comparison of stamped sheets and femoral component.

Parameter	Definition	Unit	Equation
Ra	Arithmetic average height	µm	$Ra = \frac{1}{n}\sum_{i=1}^{n}\lvert y_i\rvert$ (1)
Rq	Root mean square roughness	µm	$Rq = \sqrt{\frac{1}{n}\sum_{i=1}^{n} {y_i}^2}$ (2)
Rsk	Symmetry about the mean line	-	$Rsk = \frac{1}{NRq^3}\sum_{i=1}^{n} {y_i}^3$ (3)
Rku	Sharpness of profile's probability density	-	$Rku = \frac{1}{NRq^4}\sum_{i=1}^{n} {y_i}^4$ (4)
Rp	Maximum height of peaks	µm	$Rp = \max(y_i)$ (5)
Rv	Maximum depth of valleys	µm	$Rv = \min(y_i)$ (6)

Sofwtare Talyprofile Lite 7.1 was used to select and calculate roughness parameters. Although most SPIF works only check the surface via Ra or Rq, it is important to use other parameters to characterize the surface morphology. According to Souza Ruzzi et. al. (2020), the parameters Rsk and Rku are also widely used in manufacturing engineering, given their ability to differentiate, respectively, the predominance and spacing of peaks or valleys in profiles with similar Ra values. Still, the graphic representation of Rsk and Rku allows to observe the morphological space, proposed by Bhusan (2000), in which the appearance of the roughness profiles resulting from each manufacturing process are grouped into typical

regions, as shown in Fig. 3(a) and Fig. 3(b). Furthermore, as evidenced by Gadelmawla et. al. (2002), parameters such as Rp and Rv can help to differentiate the topography. The definitions of these parameters are shown in Tab. 2, whose values are automatically calculated in Talyprofile considering Eq. (1) to Eq. (6), for the points acquired by the rugosimeter.

3. RESULTS AND DISCUSSION

The variation of the parameters Ra, Rq, Rp and Rv can be seen in Fig. 4 and Fig. 5, while Fig. 6 shows the morphological space obtained according to Rsk and Rku for each SPIF condition. The ANOVA variance test with a confidence interval of 95% indicated that there was a statistically significant difference only in the parameters Ra ($p = 0.0015$), Rq ($p = 0\ .0030$), Rp ($p = 0.0322$) and Rv ($p = 0.0120$) for the seven stamping conditions. In order to verify which of the parameters caused this difference, the means and standard deviations were recalculated for the two levels (+ and -) of each variable (V, f, p, L), and the significance test between means was performed in Statistica 12 to verify the p values. As can be seen in Tab. 3, among the values of V, f, p and L used in the tests, the variation in the vertical step was the only statistically significant factor ($p < 0, 05$) for the change in surface roughness, with effect also on Rku in addition to Ra, Rq, Rp and Rv. This behavior is in line with that observed by Kumar et. al (2018) in the incremental stamping of AA2024 aluminum, although the authors have obtained lower average roughness, between 0.6 and 1.4 µm, thanks to the combination of low values of vertical pitch and high rotations.

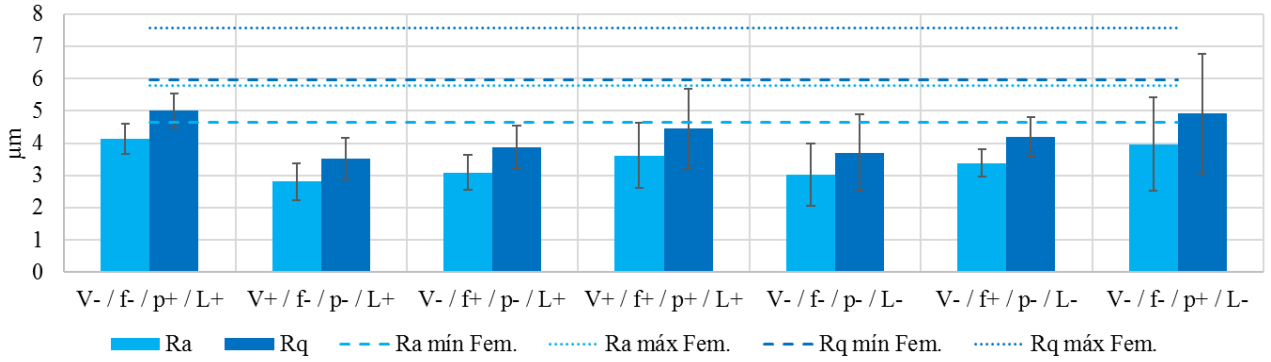

Figure 4. Ra and Rq obtained for each SPIF test and comparison with that of the femoral component of hip implant.

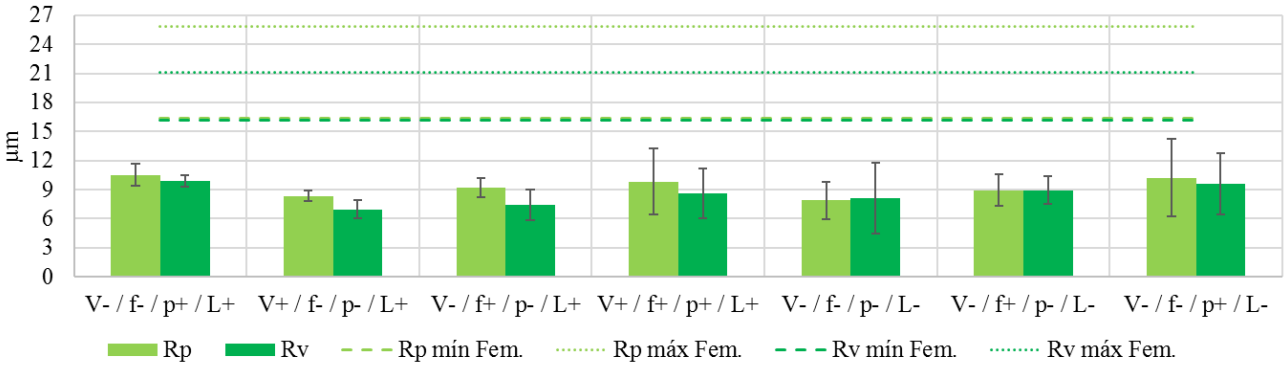

Figure 5. Rp and Rv obtained for each SPIF test and comparison with that of the femoral component of hip implant.

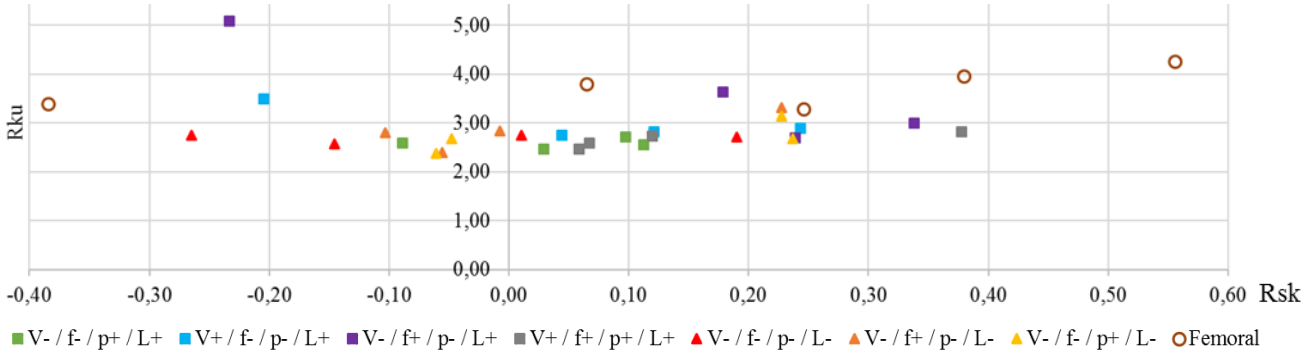

Figure 6. Morphological space for the four roughness measurements in each SPIF sample and femoral component. Triangles and squares indicate the dry and lubricated tests, respectively.

Table 3. p-values in the comparison between the levels (+ and -) of each variable for the different roughness parameters. The 5% significance level adopted requires that $p < 0.05$ for a statistically significant difference.

p-values (two-sided)	Ra	Rq	Rsk	Rku	Rp	Rv
V	0,2219	0,2321	0,4071	0,6932	0,6287	0,0843
f	0,5825	0,6654	0,3024	0,2037	0,8677	0,5682
p	0,0001	0,0001	0,3568	0,0319	0,0019	0,0032
L	0,8500	0,8649	0,2427	0,2740	0,4062	0,2461

The Ra values obtained are close to those obtained in previous works related to biomedical applications of the SPIF process. Cheng et. al. (2020) reported the production of titanium knee implants with an Ra of 5.7 µm, a value lower than that normally obtained by milling and forging. Milutinović et. al. (2021) produced stainless steel orthodontic prostheses with Ra between 3.5 and 5.5 µm. According to Deng et. al. (2015), the most beneficial Ra values for osseointegration are closer to 2.5 µm, and higher values would not improve biocompatibility. However, the commercial hip implant used as benchmark shows Ra between 4,6 and 5,8 µm, and it must be highlighted that the plasma spray technique, very common in this kind of biomedical product, typically yields higher roughness. In this sense, although tests 2 and 3 would present the most beneficial Ra for osseointegration, tests 1 and 7 show closer Ra to that of the commercial product.

Regarding Rp and Rv, it is clear that plasma spray leads to more accentuated features in comparison to SPIF, which could provide intermechanical locking with bone tissue. The impingement of the melted titanium particles is responsible for cutting and deforming the surface to create valleys while peaks are also formed when these particles solidify. Although none of the stamped parts show equivalent values for these parameters, tests 1, 4 and 7 are the closest ones. Therefore, overall, it can be said that tests 1 and 7 yield surface roughness characteristics with amplitude closest to that of the already validated femoral component.

The analysis of the morphological space indicates that the SPIF surfaces have a slight predominance of peaks ($Rsk > 0$), especially in the lubricated condition, whereas in dry tests most measurements presented more pronounced valleys. According to Han et. al. (2019), the latter is preferred because valleys are the preferential sites for cell adhesion. However, the implant surface also shows the prevalence of peaks, which is a limitation of the plasma spray process. In this sense, although lubricated tests in general yield a morphological space closer to that of the implant, the symmetry and sharpness of the profile indicated by Rsk and Rku, respectively, is even more adequate in the dry stamped parts.

With few exceptions, SPIF surfaces present high flattening ($Rku < 3$) while the Rq/Ra ratio are all around 1.23. Since Rq is more sensitive to the presence of peaks and valleys, this constant ratio and lower Rku indicate the regularity of the formed surfaces. This and the low size of the features shown by smaller Rp and Rv, mostly between 6 and 12 µm, can be associated with the deflection of the sheet along the successive movements of the tool, as in the mechanisms in Fig. 7(b) and Fig. 7(c). Indeed, the dependence of the vertical step is clear in these deformation modes, which explains why it was the only parameter with statistical significance. On the other side, random variations arise due to material plastic flow, which depends mostly on the lubrication and tool rotation. Still, this type of surface is similar to that obtained by turning, milling and EDM (Whitehouse, 2003), reinforcing the capacity of SPIF to produce ready to use biomedical parts.

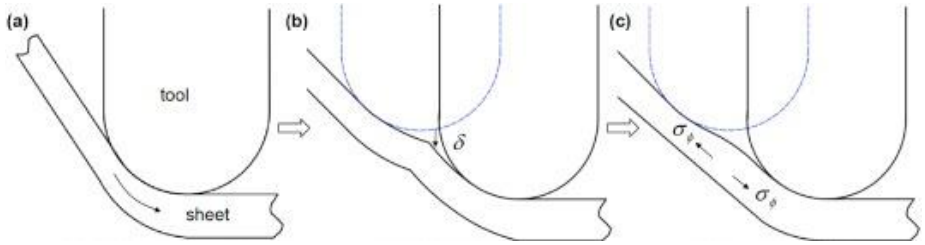

Figure 7. Deformation mechanisms of plates in the SPIF process that influence roughness. (a) Uneven thinning. (b) Bending. (c) Stretching. Adapted from Chang, Z. and Chen, J. (2019).

The topography of the plasma sprayed femoral component is shown in Fig. 8 and presents very rough aspect, which explains the high Rp and Rv observed. Again, the plasma spray process is responsible for impinging melt blocks of material onto the surface, creating a highly deformed layer that can extend up to dozens of micrometers. While the smaller valleys work as preferential site for cell adhesion due to increased contact area, the peaks also provide mechanical interlocking with the developed tissue. Additionally, the chemical analysis by EDS for this item can be seen in Fig. 9, showing an extremely high content of oxygen. As previously explained, titanium oxides promote attachment and growth of bone cells, and for that reason, plasma spray process is usually carried out with titanium dioxide particles and can be preceded by abrasive jetting with aluminum oxide, whose typically sharp particles also contribute to increasing surface roughness.

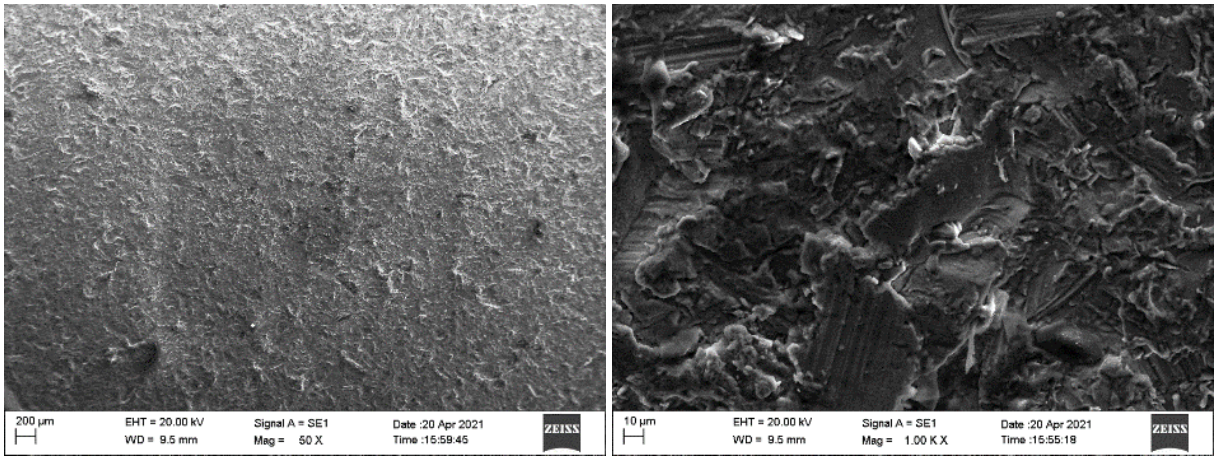

Figure 8. Topography aspect by SEM image of femoral component at 50x and 1000x.

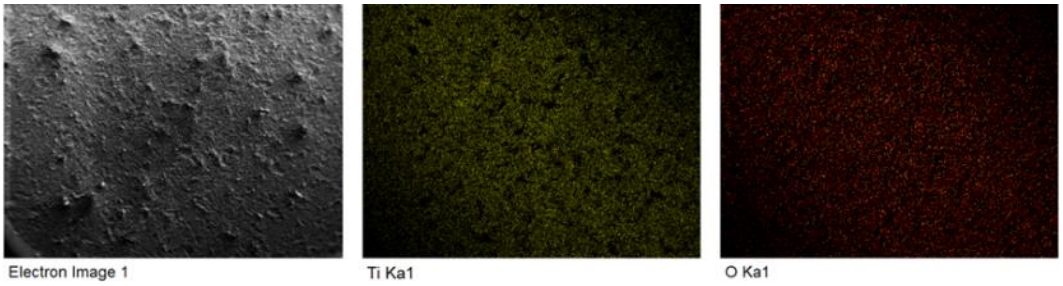

Element (% weight)	
Ti	O
54.24	46.05

Figure 9. Chemical composition and element map by EDS and SEM of femoral component (50x).

Figure 10 shows the internal surface of the cone produced in test 5, for lower rotation, feed and vertical step at dry condition. There is a clear occurrence of plastic flow at the microscale as indicated by the circles in Fig. 10(b), which causes the rough aspect at macroscale seen in Fig. 10(a). According to Hussain et. al. (2012), shear at the interface between sheet and tool generates localized heat, which contributes to greater material deformability. This is especially important for titanium, which has low plasticity at room temperature.

The peaks and valleys are not as pronounced as in the plasma sprayed component, in agreement with the lower values for Rp and Rv in the formed parts. Again, this has to do with the deformation mechanisms that govern the Single Point Incremental Sheet Forming process, shown in Fig. 7. While the smaller vertical step yields lower roughness, the absence of lubricant increases friction and leads to random material flow in the tool interface. It becomes evident that even when tool rotation is lower, the feed speed provides enough shearing at the interface to create the rough aspect observed. That is confirmed by the greater asperity of the cone produced in test 6, for lower rotation and vertical step, but higher feed at dry condition. Besides the increase of Ra, Rq, Rp and Rv compared to test 5, the surface is even more rough as can be seen in Fig. 12, which can be attributed to the higher shear rate.

The contrary happens in the lubricated tests, which present lower roughness values overall when comparing for the same vertical step. The surface aspect becomes smoother, as shown in Fig. 16. Although there is still plastic flow, the tool tends to slide against the surface and create the marks pointed in Fig. 16(b), which are different from those obtained in dry condition. In the case of test 7, whose internal surface is shown in Fig. 14, the aspect is less rough than in the other dry tests due to lower tool rotation and feed. However, the higher vertical step creates wrinkles in the sheet due bending effect of Fig. 7(b), which explains the higher Ra and Rq for this condition. However, it is noted that none of the SPIF surfaces shows the same shape for the asperities as those from plasma sprayed implant at Fig. 8, even when roughness values are close. Overall, this could lead to lesser mechanical interlocking with newly formed bone after implantation, indicating the still better capabilities of the plasma spray treatment.

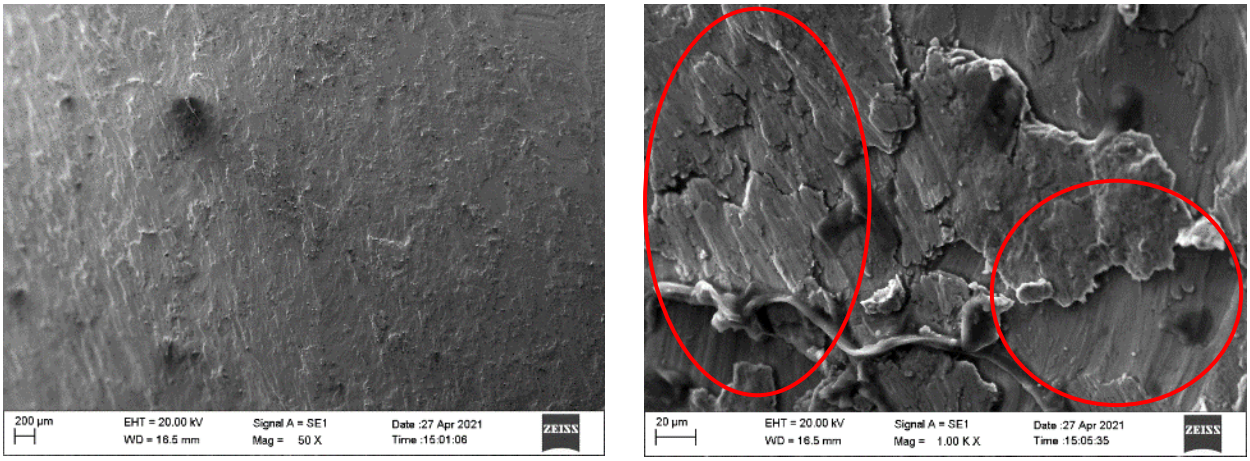

(a) (b)

Figure 10. Topography aspect by SEM image of cone from test 5 (V- / f- / p- / L-) at (a) 50x and (b) 1000x.

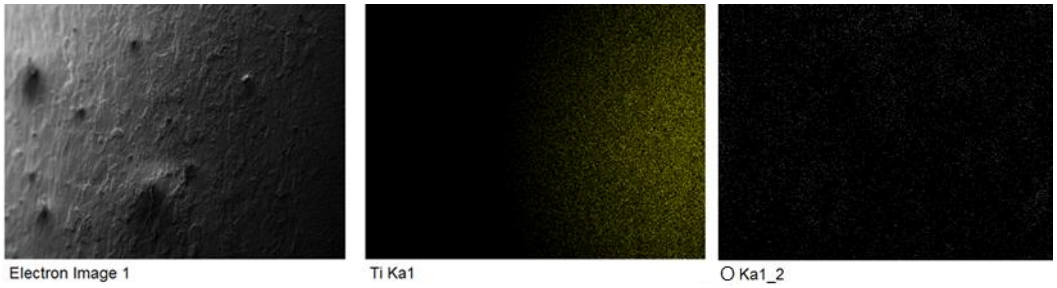

Element (% weight)	
Ti	O
95.41	2.87

Figure 11. Chemical composition and element map by EDS and SEM of cone from test 5 (V- / f- / p- / L-), at 50x.

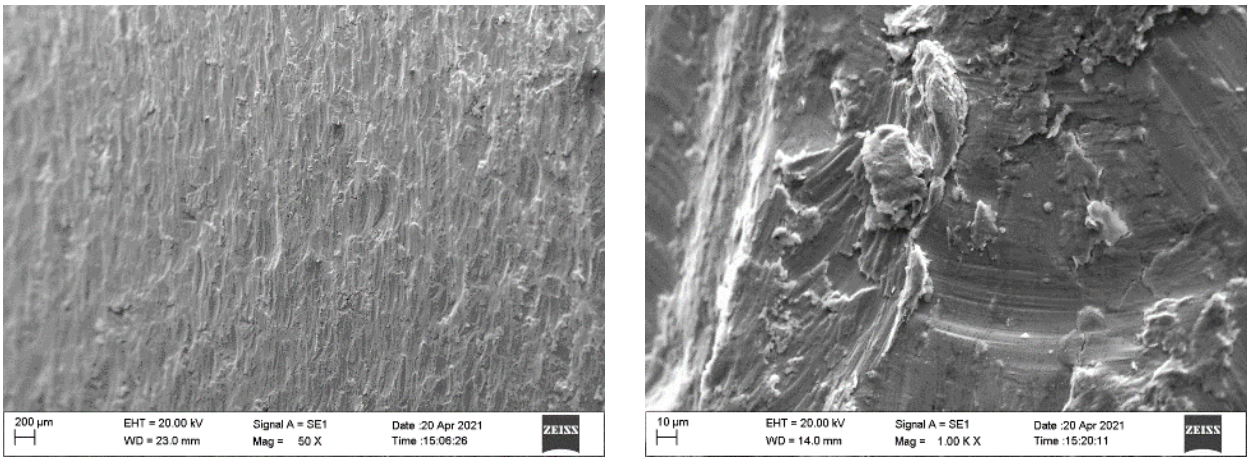

(a) (b)

Figure 12. Topography aspect by SEM image of cone from test 6 (V- / f+ / p- / L-) at (a) 50x and (b) 1000x.

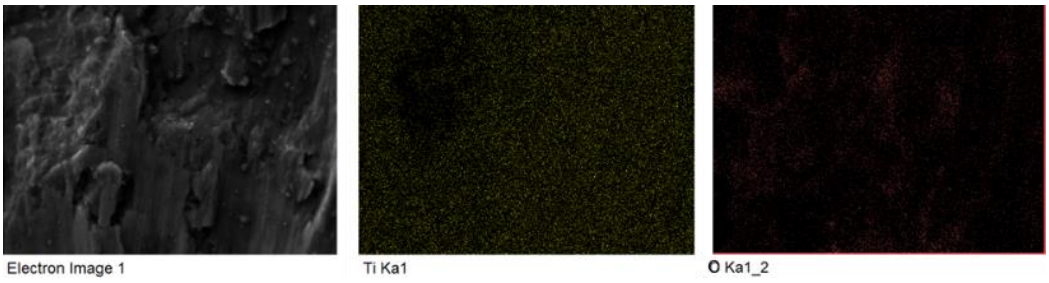

Element (% weight)	
Ti	O
93.22	5.19

Figure 13. Chemical composition and element map by EDS and SEM of cone from test 6 (V- / f+ / p- / L-), at 5000x.

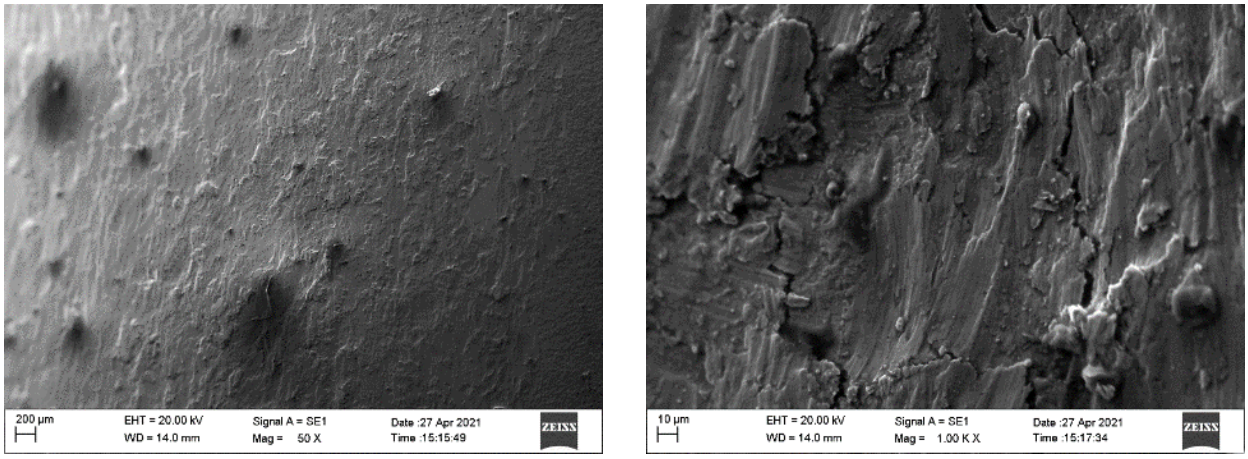

(a) (b)

Figure 14. Topography aspect by SEM image of cone from test 7 (V- / f- / p+ / L-) at (a) 50x and (b) 1000x.

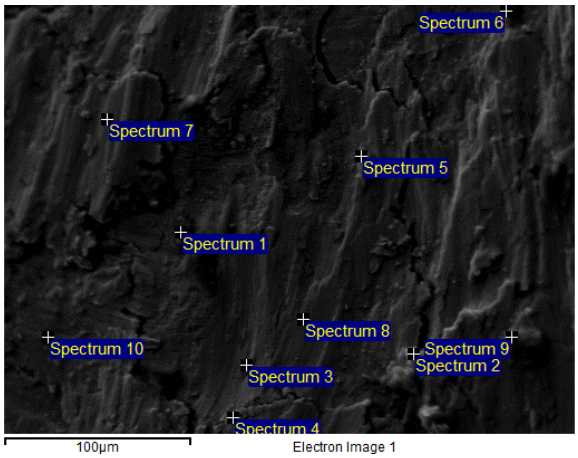

Element (% weight)	O	Ti
Spectrum 1	49.83	48.62
Spectrum 2	8.68	90.25
Spectrum 3	2.17	97.36
Spectrum 4	4.62	94.76
Spectrum 5	22.51	74.15
Spectrum 6	23.22	71.12
Spectrum 7	0.84	99.07
Spectrum 8	2.43	96.75
Spectrum 9	30.13	17.28
Spectrum 10	3.87	94.35

Figure 15. Chemical composition in different points by EDS and SEM of cone from test 7 (V- / f- / p+ / L-), at 1000x.

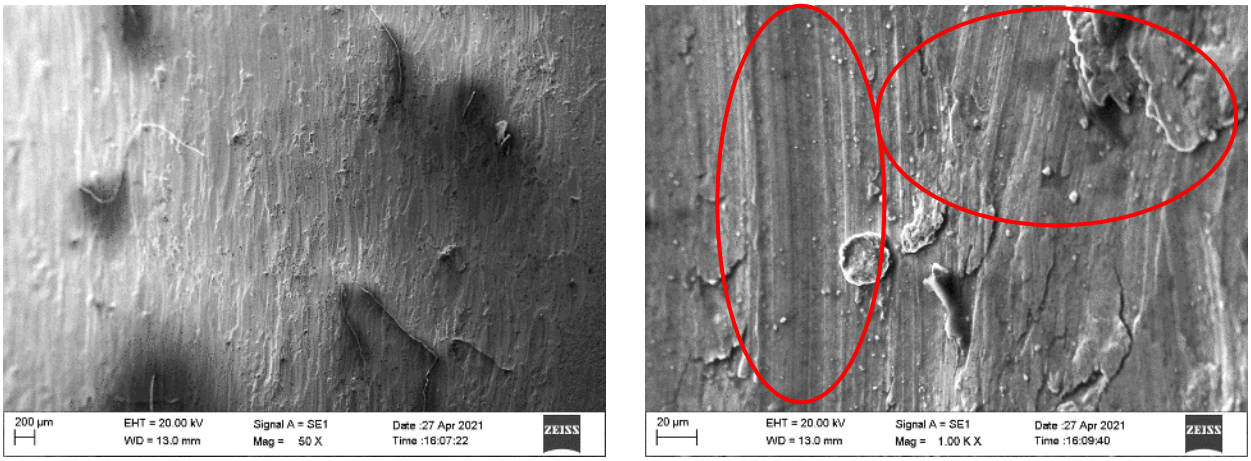

(a) (b)

Figure 16. Topography aspect by SEM image of cone from test 2 (V+ / f- / p- / L+) at (a) 50x and (b) 1000x.

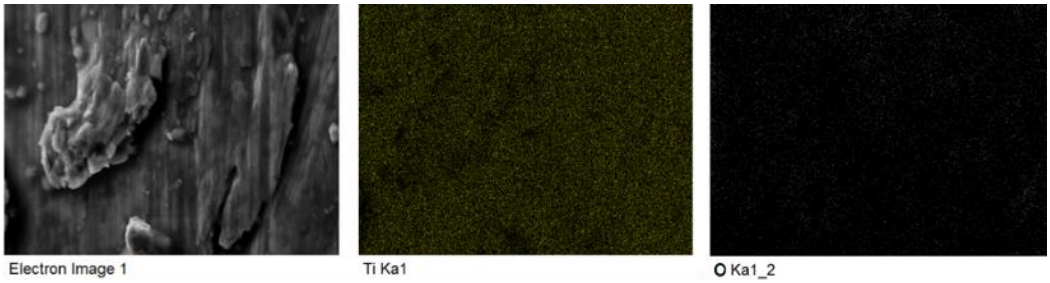

Element (% weight)	
Ti	O
96.86	1.54

Figure 17. Chemical composition and element map by EDS and SEM of cone from test 2 (V+ / f- / p- / L+), at 5000x.

Regarding the chemical composition of the surfaces produced by SPIF, the chemical analysis by EDS and element maps are shown in Fig. 11, Fig. 13, Fig. 15 and Fig. 17 for the cones produced in tests 5 (V- / f- / p- / L-), 6 (V- / f+ / p- / L-), 7 (V- / f- / p+ / L-) and 2 (V+ / f- / p- / L+), respectively. While titanium is obviously the predominant element and covers the whole surface, oxygen content is very low, but it is still present. In the incremental process, there might occur chemical reactions that lead to the formation of oxides and other compounds due to the high heat in the tool-sheet interface, especially in high friction conditions (Campos et. al., 2020). Therefore, since the sheet material is commercially pure titanium, it is likely that the heat and plastic deformation inherent to SPIF also creates titanium dioxides particles of some sort. For instance, the analysis of Fig. 15 shows points with higher prevalence of oxygen over certain spherical particles. These may come from oxidized wear particles removed from the sheet that then embed at the plastically deformed outer layer. Other possibility is the reaction of the titanium surface exposed after each pass of the tool. Indeed, it should be noted that the O content is greater in the cones obtained at dry condition, since oxidation of the sheet or wear particles would be favored without the protection from the lubricant. This phenomenon would also be favored by the greater shear rate from test 6, due to the higher feed. This is in line with the higher oxide content observed for this test condition in Fig. 13.

Differently from what was observed in the plasma sprayed commercial implant, the formation of titanium oxides is severely reduced, given the much lower oxygen content. In addition, instead of a thick homogeneous layer, the oxides appear as localized spherical particles spread non-uniformly at the surface. Although this is less beneficial for osseointegration, it is known that titanium exposed to air naturally forms an oxide layer of TiO_2 in at least a few tens of nanometers (Chen et. al., 2020), which is hardly captured in the EDS spectrum, whose signal predominantly reflects the chemical composition of the region between 1 and 2 µm below the surface. Therefore, even though the chemical composition at the surface of the parts produced by SPIF might be significantly different from those of the current biomedical products, it is very likely that the biological properties are conserved. Together with the beneficial cell activity in surfaces with lower Ra (Deng et. al., 2015), these characteristics could indicate suitability of the SPIF process to produce implants without the need for subsequent processes such as plasma spray.

4. CONCLUSIONS

Single Point Incremental Sheet Forming tests were carried on titanium sheets under 7 different conditions. The roughness was assessed by different parameters, while SEM images and chemical composition analysis by EDS were used to compare surface characteristics to that of a commercial hip implant. The following conclusions could be verified:

• The main process variable towards roughness was the vertical step, with a statistically significant influence on the parameters Ra, Rq, Rku, Rp and Rv;

• The most adequate Ra values for cell proliferation according to previous studies were obtained in tests 2 and 3, but tests 1 and 7 yielded closest Ra to that of the femoral component of the validated implant;

• The analysis of the morphological space (combination of Rsk and Rku) indicated that the surfaces predominantly present peaks with intermediate flattening in the femoral implant and cones of the lubricated tests, while valleys were predominant in the dry tests;

• Considering the distribution of peaks and valleys, the most suitable parameters for biomedical applications were obtained in tests 5, 6 and 7. Although the literature recommends lower Ra as in obtained in dry tests, the higher Ra of the commercial implant is closer to that of test 7, making its process parameters the best choice in Incremental Forming o Ti;

• The surface characteristics obtained by SPIF are close to those produced by turning, EDM and some cases of milling, indicating the capacity of the SPIF process to replace them in the manufacture of certain implants regarding surface finish;

• SEM images and EDS analysis revealed regions of high material plastic flow with embedded titanium dioxide particles. The TiO_2 content was higher in dry tests due to easier oxidation of wear particles and Ti sheet;

Despite the uneven distribution of titanium oxide fragments on the surface and lower amount compared to the plasma sprayed femoral component, these structures are still present, which guarantees the biocompatibility of the formed parts and indicate the ability of the SPIF process to produce ready to use biomedical parts.

5. ACKNOWLEDGEMENTS

The authors are thankful to CNPq, FAPEMIG and CAPES (Funding Code 01) for fostering postgraduate scholarships, to the Multiuser Microscopy Laboratory of the Faculty of Chemical Engineering, the Metrology Teaching Laboratory and the Machining Teaching and Research Laboratory of the Federal University of Uberlândia for the support in carrying out the tests.

6. REFERENCES

Agarwal, R. e García, A. J., 2015. "Biomaterial strategies for engineering implants for enhanced osseointegration and bone repair". *Advanced drug delivery reviews*, Vol. 94, p. 53-62.

Bhushan, B., 2000. *Modern tribology handbook 1. Principles of tribology*. CRC press, Boca Raton, 1st ed.

Campos, F. A. R., Souza, F. C. R., Silva, L. R. R. e França, P. H. P., 2020. "Study of different lubri-coolant conditions for incremental sheet forming of thin zinc sheets". *A Aplicação do Conhecimento Científico na Engenharia Mecânica*, Vol. 1, p. 21-34.

Oliveira, B. J., da Silva, L. R. R., Campos, F. A. R., França, P. H. P., Mateus, V. v. G., Barreto, J. C. N. and Sales, W. F. (2018). "Análise da velocidade de avanço na estampagem incremental do aço AISI 304". *Sciencomm Online*, Vol. 8, p. 14-22.

Chang, Z. e Chen, J., 2019. "Analytical model and experimental validation of surface roughness for incremental sheet metal forming parts". *International Journal of Machine Tools and Manufacture*, Vol. 146, 103453.

Chen, C. S., Chang, J. H., Srimaneepong, V., Wen, J. Y., Tung, O. H., Yang, C. H., Lin, H. C., Lee, T. H., Han, Y. e Huang, H. H., 2020. "Improving the in vitro cell differentiation and in vivo osseointegration of titanium dental implant through oxygen plasma immersion ion implantation treatment". *Surface and Coatings Technology*, Vol. 399, 126125.

Cheng, Z., Li, Y., Xu, C., Liu, Y., Ghafoor, S. e Li, F., 2020. "Incremental sheet forming towards biomedical implants: a review". *Journal of Materials Research and Technology*, Vol. 9, No. 4, p. 7225-7251.

Civantos, A., Domínguez, C., Pino, R. J., Setti, G., Pavón, J. J., Martínez-Campos, E., Garcia, F. J. G., Rodríguez, J. A., Allain, J. P. e Torres, Y., 2019. "Designing bioactive porous titanium interfaces to balance mechanical properties and in vitro cells behavior towards increased osseointegration". *Surface and Coatings Technology*, Vol. 368, p. 162-174.

Deng, Y., Liu, X., Xu, A., Wang, L., Luo, Z., Zheng, Y., Deng, F., Wei, J., Tang, Z. e Wei, S., 2015. "Effect of surface roughness on osteogenesis in vitro and osseointegration in vivo of carbon fiber-reinforced polyetheretherketone–nanohydroxyapatite composite". *International journal of nanomedicine*, Vol. 10, p. 1425.

Doss, Q. M., Abaas, T. F., & Bedan, A. S. (2013). An investigation study of thinning distribution in single point incremental forming using FEM analysis. Al-Khwarizmi Engineering Journal, 9(3), 1-14.

Gadelmawla, E. S., Koura, M. M., Maksoud, T. M. A., Elewa, I. M. e Soliman, H. H., 2002. "Roughness parameters". *Journal of materials processing Technology*, Vol. 123, Ed. 1, p. 133-145.

Gandla, P. K., Inturi, V., Kurra, S. e Radhika, S., 2020. "Evaluation of surface roughness in incremental forming using image processing based methods". *Measurement*, Vol. 164, 108055.

Hacking, S. A., Boyraz, P., Powers, B. M., Sen-Gupta, E., Kucharski, W., Brown, C. A. e Cook, E. P., 2012. "Surface roughness enhances the osseointegration of titanium headposts in non-human primates". *Journal of neuroscience methods*, Vol. 211, No. 2, p. 237-244.

Han, X., Yang, D., Yang, C., Spintzyk, S., Scheideler, L., Li, P., Li, D., Geis-Gerstofer, J. e Rupp, F., 2019. "Carbon fiber reinforced PEEK composites based on 3D-printing technology for orthopedic and dental applications". *Journal of clinical medicine*, Vol. 8, No. 2, p. 240.

Hussain, G., Gao, L., Hayat, N., Cui, Z., Pang, Y. C. e Dar, N. U., 2008. "Tool and lubrication for negative incremental forming of a commercially pure titanium sheet". *Journal of Materials Processing Technology*, Vol. 203, p. 193-201.

ISO 4288, 2008. "Geometrical Product Specifications (GPS)--surface Texture: Profile Method--rules and Procedures for the Assessment of Surface Texture". *International Organization for Standardization*.

Kumar, A., Gulati, V. e Kumar, P., 2018. "Investigation of surface roughness in incremental sheet forming". *Procedia computer science*, Vol. 133, p. 1014-1020.

Mateus, V. v. G., da Silva, L. R. R., Carvalho, L. P. and Sales, W. F. (2018). "Processo de estampagem incremental em chapas de aço aisi 316". *In Proceedings of the XXV National Congress of Mechanical Engineering Students-CREEM2018*, Brasília.

7. RESPONSIBILITY NOTICE

The authors are the only responsible for the printed material included in this paper.